INSTITUTE OF PHYSICS PUBLISHING NANOTECHNOLOGY
Nanotechnology **17** (2006) 758–762 doi:10.1088/0957-4484/17/3/024

Observation of gain-coupled distributed-feedback effects in V-groove InGaAs/AlGaAs quantum-wire arrays

Tae Geun Kim[1,2], **Yasuhide Tsuji**[3] **and Mutsuo Ogura**[2]

[1] Department of Electronics Engineering, Korea University, Seoul 136-701, Korea
[2] National Institute of Advanced Industrial Science and Technology, Tsukuba, Ibaraki 305-8568, Japan
[3] Department of Electrical and Electronics Engineering, Kitami Institute of Technology, Hokkaido, Japan

E-mail: tgkim1@korea.ac.rk

Received 7 September 2005
Published 10 January 2006
Online at stacks.iop.org/Nano/17/758

Abstract
InGaAs/AlGaAs V-groove quantum-wire (QWR) arrays were fabricated by holographic lithography and one-time metalorganic chemical vapour deposition (MOCVD) to evaluate gain-coupled distributed-feedback (GC-DFB) effects in the InGaAs/AlGaAs materials. Using a finite-element method (FEM), mode analysis of the actual cross-sectional structure verified the modal gain of the QWR DFB structure, in which the gain was identified by a single peak at the Bragg wavelength of the grating. In addition, we observed a large gain anisotropy due to the gain/loss coupling in the DFB structure at a wavelength of 914 nm in the emission spectra from the 430 nm pitch QWR grating at room temperature.

1. Introduction

Integration of semiconductor nanostructures with conventional optoelectronic devices has been attempted to improve device performance [1, 2]. An interesting semiconductor laser is the quantum-wire (QWR) gain-coupled distributed-feedback (GC-DFB) laser [3, 4] fabricated by combining a DFB laser and a V-groove QWR array. By adjusting the DFB periodicity to V-groove QWR gain, researchers have been able to fully apply the advantages of QWRs without being concerned about the parasitic sidewall quantum wells (SQWs). The feasibility of these devices was proven experimentally [4, 5] but has not been confirmed at room temperature (RT). Perturbed waveguide structures as well as the increase in trap densities (at the interface between the surface of the grating and the epitaxial layer grown on it) by grating overgrowth are regarded as the main obstacles to RT investigation.

We have reported a constant metalorganic chemical vapour deposition (MOCVD) growth technique able to preserve the grating profiles even after the growth of 1 μm thick AlGaAs lower cladding layers as a means of solving the overgrowth problem [6]. Using this technique and reducing the interface density, we obtained GaAs/AlGaAs GC-DFB lasers that could be operated at RT. However, in this GaAs/AlGaAs materials system the gain effects of the GC-DFB laser were not observed, although it lased at a very low threshold current. This was then attributed to insufficient gain modulation between the QWRs and SQWs due to the limited diffusion length of gallium in V-groove GaAs/AlGaAs QWRs [7].

In this work we observed distributed optical feedback via gain coupling in directions perpendicular to the V-groove in $In_{0.2}Ga_{0.8}As/Al_{0.2}Ga_{0.8}As$ QWR arrays. The structure was grown by using a constant MOCVD growth technique to reduce interface-related non-radiative recombination. Using a finite-element method (FEM), mode analysis of the QWR DFB structure against emission wavelength showed a single modal gain near the Bragg wavelength of the grating. The emission spectra taken at RT for the DFB direction of the QWR array showed a single gain peak at 914 nm near the Bragg wavelength as evidence of the GC-DFB effects.

The $In_{0.2}Ga_{0.8}As/Al_{0.2}Ga_{0.8}As$ QWR GC-DFB laser was grown by low-pressure MOCVD on a V-groove array (0.43 μm pitch and 0.2 μm depth) of GaAs. The grating was fabricated by holographic photolithography and chemical wet etching. The laser structure, as shown in figure 1, consisted of a 0.1 μm thick n-GaAs buffer layer, a 0.9 μm thick

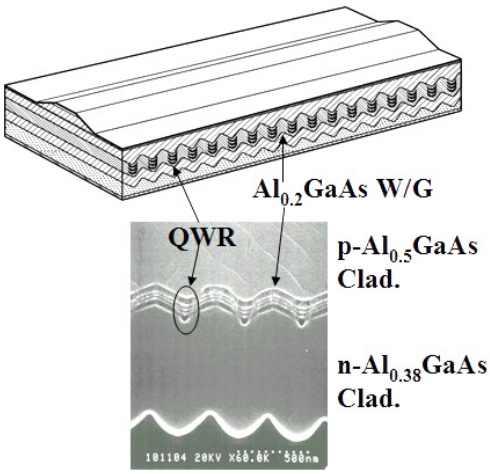

Figure 1. Schematic diagram (top) and cross-sectional SEM image (bottom) of the QWR GC-DFB laser.

n-$Al_{0.38}Ga_{0.62}As$ lower cladding layer, a 0.1 μm thick undoped $Al_{0.2}Ga_{0.8}As$ guiding layer, three 5 nm-thick $In_{0.2}Ga_{0.8}As$ QWs separated by two undoped 10 nm thick $Al_{0.2}Ga_{0.8}As$ barrier layers, a 0.1 μm thick undoped $Al_{0.2}Ga_{0.8}As$ guiding layer, a 1 μm thick p-$Al_{0.5}Ga_{0.5}As$ upper cladding layer and a 0.2 μm thick GaAs p+ contact layer from the bottom. Epitaxial growth was carried out in a horizontal quartz reactor using a facedown configuration of the wafer by means of a low-pressure MOCVD technique at 76 Torr. Triethylgallium, trimethylaluminium, trimethylindium and AsH_3 were used as the source reagents and the V/III ratio was 200. The indium content was measured by energy dispersive spectroscopy. A cross-sectional image (see figure 1) of the laser observed by a high-resolution scanning electron microscope (HR-SEM) showed that the three crescent-shaped $In_{0.2}Ga_{0.8}As/Al_{0.2}Ga_{0.8}As$ QWRs were well formed on the 0.9 μm thick n-doped $Al_{0.38}Ga_{0.62}As$ cladding layer without any regrowth process. The size of each QWR determined by a transmission electron microscope (TEM) was 8 nm thick and 80 nm wide, and the photoluminescence (PL) wavelength observed from the QWRs was 915 nm at RT in our previous work [7]. In addition, unlike the GaAs/AlGaAs case [5], a strong and well-separated PL spectrum from the SQW was observed from the QWR region even at RT, indicating that the $In_{0.2}Ga_{0.8}As/Al_{0.2}Ga_{0.8}As$ QWR array is more suitable for observing the QWR GC-DFB effects.

2. Mode analysis of the V-groove QWR and DFB structure

First, the complex propagation coefficient γ of the present laser structure was numerically calculated to investigate the change in the propagation mode with respect to the emission wavelength. In general, the coupled wave equation has been used for the analysis of the DFB grating; however, it is not suitable for the present QWR GC-DFB laser structure since our laser structure has a perturbed waveguide composed of a QWR array. Therefore, we used a specially designed finite-element analysis [8, 9] based on the actual cross-sectional structure of

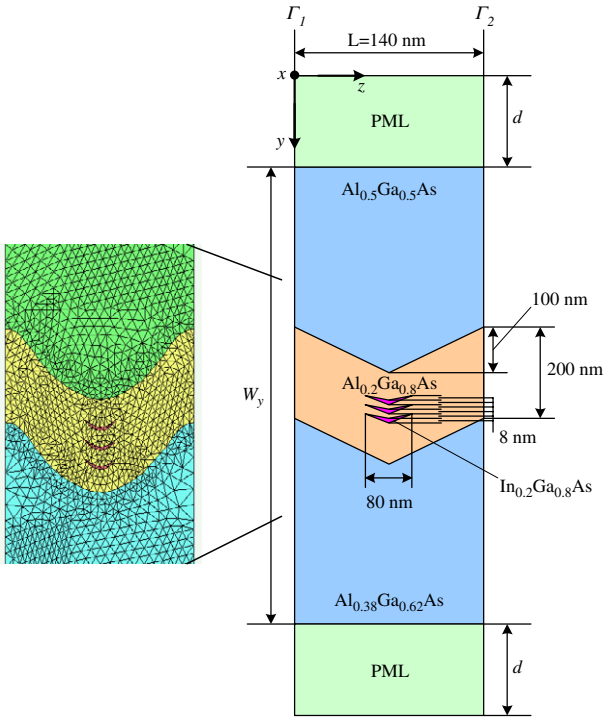

Figure 2. Unit cell of the InGaAs/AlGaAs QWR GC-DFB structure for the mode analysis.
(This figure is in colour only in the electronic version)

the QWR GC-DFB structure for more precise calculation of the γ.

Figure 2 shows a unit cell structure of the QWR GC-DFB laser that was used in the mode analysis. The complex refractive index n_c $(= n + jg)$ was assumed in the active QWR region, where n is the refractive index of the index gratings and g is the refractive index of the gain gratings. The dimensions of each component of the DFB structure shown in figure 2 were determined from the cross-sectional TEM image. To reduce the size of the computational window and suppress the spurious coupling between the guided mode and radiation mode, an anisotropic perfectly matched layer (PML) [8–10], reported as an effective boundary condition for assuming the infinite region of the model, was used at the upper and lower boundaries.

From Maxwell's equation, a scalar wave equation for 2D analysis of the DFB structure is given by

$$\frac{\partial}{\partial y}\left(p_y \frac{\partial \Phi}{\partial y}\right) + \frac{\partial}{\partial z}\left(p_z \frac{\partial \Phi}{\partial z}\right) + k_0^2 q \Phi = 0 \qquad (1)$$

with

$$\Phi = \begin{cases} E_x \quad p_y = s \quad p_z = \dfrac{1}{s} \quad q = sn_c^2 \\ \quad \text{for the TE mode} \\ H_x \quad p_y = \dfrac{s}{n_c^2} \quad p_z = \dfrac{1}{sn_c^2} \quad q = s \\ \quad \text{for the TM mode} \end{cases} \qquad (2)$$

where E_x and H_x are the x components of the electric and the magnetic fields, respectively, n_c is the complex refractive

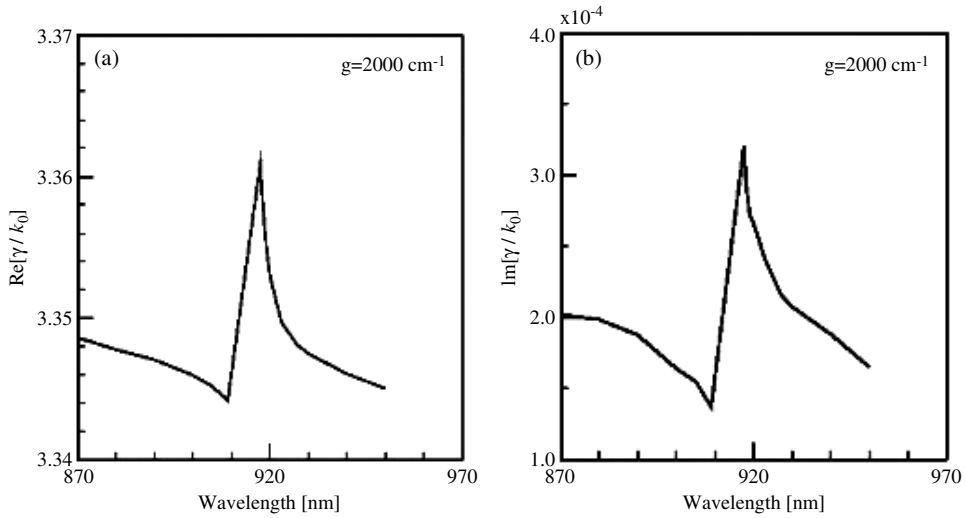

Figure 3. (a) Real and (b) imaginary parts of the complex propagation constant γ against wavelength when the gain distribution of the medium is assumed to be proportional to the probability of the electrons at the first subband level.

index, k_0 is the free-space wavenumber and s is the PML parameter, which is a real or complex value according to whether the eigenmode is a guided mode or a leaky mode.

Assuming a z-propagating optical field with a complex propagation coefficient $\gamma = \beta + \mathrm{j}\alpha$, where β indicates the effective index and α indicates the normalized modal gain, the field can be expressed as

$$\Phi(y, z) = \phi(y, z)\exp(-\mathrm{j}\gamma z) \tag{3}$$

and by substituting (3) into (1), (1) is rewritten as

$$\frac{\partial}{\partial y}\left(p_y\frac{\partial\phi}{\partial y}\right)+\frac{\partial}{\partial z}\left(p_z\frac{\partial\phi}{\partial z}\right)-2\mathrm{j}p_z\gamma\frac{\partial\phi}{\partial z}+(k_0^2q-p_z\gamma^2)\phi=0. \tag{4}$$

Then, by applying the standard FEM to (4) and by using the periodic boundary conditions to the left and right boundaries as in (5) and (6),

$$\Phi|_{\Gamma_2} = \exp(-\mathrm{j}\gamma L)\Phi|_{\Gamma_1} \tag{5}$$

$$p_z\frac{\partial\Phi}{\partial z}\bigg|_{\Gamma_2} = \exp(-\mathrm{j}\gamma L)p_z\frac{\partial\Phi}{\partial z}\bigg|_{\Gamma_1} \tag{6}$$

we can obtain the following eigenvalue equation:

$$([K(\gamma)]-\gamma^2[M])\{\phi\} = \{0\} \tag{7}$$

with

$$\{\phi\}_{\Gamma_2} = \{\phi\}_{\Gamma_1} \tag{8}$$

$$[K(\gamma)] = \sum_e\int\int_e\Bigg[-p_y\frac{\partial\{N\}}{\partial y}\frac{\partial\{N\}^{\mathrm{T}}}{\partial y}-p_z\frac{\partial\{N\}}{\partial z}\frac{\partial\{N\}^{\mathrm{T}}}{\partial z} - \mathrm{j}\gamma p_z\left(\frac{\partial\{N\}}{\partial z}\{N\}^{\mathrm{T}}-\{N\}\frac{\partial\{N\}^{\mathrm{T}}}{\partial z}\right) + k_0^2q\{N\}\{N\}^{\mathrm{T}}\Bigg]\mathrm{d}y\,\mathrm{d}z \tag{9}$$

$$[M] = \sum_e\int\int_e p_z\{N\}\{N\}^{\mathrm{T}}\,\mathrm{d}y\,\mathrm{d}z \tag{10}$$

where $[K]$ and $[M]$ are the matrices used as the FEM finally reduces to a matrix calculation, and $\{N\}$ is the column vector called 'shape function' in the FEM. This nonlinear generalized complex eigenvalue problem can be solved self-consistently by using an appropriate initial value of γ in (9). The initial value of γ is obtained by solving the linear generalized eigenvalue equation with respect to γ^2, and again assigning the obtained value into γ of $[K(\gamma)]$ in formula (7). The same calculation process is then repeated and finally the solution to the nonlinear generalized eigenvalue problem (7) is achieved by choosing the convergent solution of γ. For reference, the initial value of γ can be converged in a waveguide mode by defining the maximum refractive index of the waveguide region as '$n_$max' and by getting '$\gamma = k_0 \times n_$max'. This value is merely an initial value and therefore it has a certain allowance. Numerical results shown in figure 3 are discontinuous in the regions near the gain peak and gain valley since the solution was not converged well in this range due to limited resolution in the analysis.

3. Results and discussion

Figures 3(a) and (b) show the real part of the propagation constant $\mathrm{Re}[\gamma/k_0]$ (i.e. effective index β/k_0) spectrum and the imaginary part of the propagation constant $\mathrm{Im}[\gamma/k_0]$ (i.e. normalized modal gain α/k_0) spectrum, calculated against wavelength when the gain distribution of the medium is assumed to be proportional to the probability of the existence of an electron at the first subband level. Peak gain was normalized to be 2000 cm^{-1}. To determine the subband spacing of the QWR, the electronic state of the QWR was calculated by solving the 2D single-band Schrödinger equation [11]. In figure 3, both refractive index and gain index varied with wavelength, in which the dip and peak of the refractive index coincided with those of the gain at 910 and 918 nm, respectively. These coincidences seem reasonable because the periodicity of the gain grating is in phase with that of the index grating in the present QWR GC-DFB structure. The dispersion

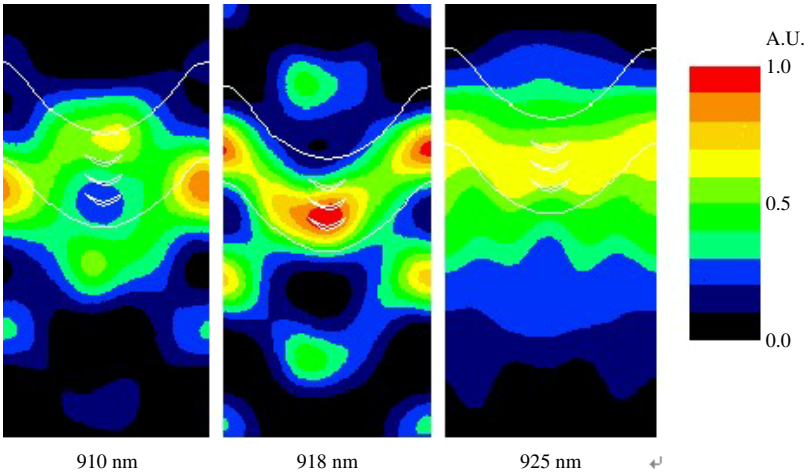

Figure 4. Optical field distributions calculated at wavelengths of 910, 918 and 925 nm.

gain curve was changed from index coupling to gain coupling by varying the gain constant g, as in the case of GaAs/AlGaAs QWR lasers.

As shown in figure 4, the optical field distributions against wavelength for $g = 2000\,\mathrm{cm}^{-1}$ were also simulated by solving the well-known field equation [8, 9]. We normalized the intensity of the optical field in all three parts of figure 4 to see how the field overlaps with QWRs. The V-groove QWR array was schematically shown with black lines and the intensity of the field was expressed in a different colour scale. It appears that in figure 4(a) the field is weakly confined in the QWR array at 910 nm while in figure 4(b) it is strongly confined in the QWR array at 918 nm. This result is interestingly consistent with the result of the modal gain analysis with a dip and peak profile at 910 and 918 nm, respectively (see figure 3(b)). In figure 4(c), it appears there is a larger overlap between the field and the QWR array, but the field intensity is as low as one-half of the peak intensity of figure 4(b) and not confined to the QWR array. This is because the effect of the grating is averaged out along the waveguide at a wavelength of 925 nm. In contrast, in figure 4(b) although the overlap is only with two of the three QWRs, the field intensity is so high that the laser experiences higher gain as it can stimulate more carrier recombination. The fact that a single modal gain is observed (at the Bragg wavelength of the grating) only when an antinode of the optical field overlaps with the QWR array is firm evidence showing that the present QWR laser operates by distributed optical feedback using a QWR gain grating.

Figure 5 show the emission spectra from the InGaAs/AlGaAs QWR GC-DFB structure with a 500 μm long cavity. Tests were carried out under RT pulsed operation with a pulsewidth of 1 μs and a duty of 0.1%. The threshold current was estimated to be about 50 mA, and the emission wavelength was observed to be 914 nm. Evolution of the emission spectra was investigated by increasing the current from below to near threshold to observe the changes in the gain profile. We observed large gain anisotropy in the emission spectra with a crest at a wavelength of 914 nm and a valley at a wavelength of 910 nm, reasonably consistent with the simulation results of figure 3. The gain anisotropy rapidly became large when the current increased up to 50 mA, and gradually saturated at

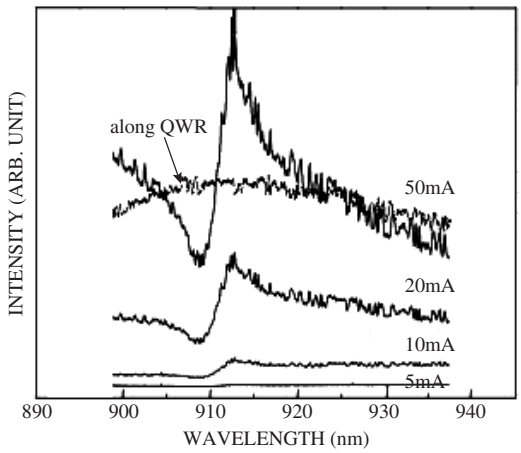

Figure 5. The emission spectra at different current levels.

currents above 50 mA. This might have been due to carrier diffusion out of the shallow ridge of the laser in the direction of the wire. Further investigation is required to clarify the exact reason this. This spectral evolution at the longer wavelength side is likely to be due to the structure of our laser, in which the gain and index grating are in phase. In DFB lasers with an index-coupling coefficient higher than the gain-coupling coefficient, it is well known that the lasing mode should be in the longer-wavelength side of the stopband of the Bragg grating, and this fact is known as the gain-matching effect [12–14]. In contrast, broad and isotropic emission spectra were observed from the laser fabricated with a stripe contact parallel to the QWR array, in which optical feedback would be produced along the QWR axis by the cavity. A typical emission spectrum measured at 50 mA along the QWR direction using Fabry–Perot modes is shown by 'along QWR' in figure 5.

4. Conclusion

We demonstrated the effect of distributed optical feedback via gain coupling from a V-groove $In_{0.2}Ga_{0.8}As/Al_{0.2}Ga_{0.8}As$ QWR array theoretically and experimentally. Asymmetric

emission with a single modal gain was observed near the Bragg wavelength of the QWR grating at RT, which corresponded to the simulation result obtained from the SEM cross-section of the QWR DFB structure using FEM. Greatly reduced interface densities throughout constant MOCVD growth and sufficient gain modulation in the DFB direction are considered to be responsible for the RT observation of the GC-DFB effects in these structures.

Acknowledgments

The authors acknowledge Dr C S Son of Silla University for his technical assistance. This work was partly supported by KOSEF through q-*Psi* at Hanyang university, Korea.

References

[1] Zah C E *et al* 1993 *Electron. Lett.* **29** 857
[2] Tiwari S, Pettit G D, Milkove K R, Legoues F, Davis R J and Woodall J M 1994 *Appl. Phys. Lett.* **64** 3536
[3] Robadey J *et al* 1997 *IEEE Photon. Technol. Lett.* **9** 5
[4] Toda T, Reinhardt F, Martinet E, Kapon E and Nakano Y 1999 *IEEE Photon. Technol. Lett.* **11** 1530
[5] Kim T G, Son C S, Tsurumachi N, Oh D K and Ogura M 2005 *Nanotechnology* **16** 1245
[6] Kim T G, Son C S and Ogura M 2001 *IEEE Photon. Technol. Lett.* **13** 409
[7] Tsurumachi N, Son C S, Kim T G, Takasuda Y and Ogura M 2002 *Japan. J. Appl. Phys.* **41** 2679
[8] Tsuji Y and Koshiba M 2002 *IEEE J. Lightwave Technol.* **20** 463
[9] Tsuji Y and Koshiba M 2000 *IEEE J. Lightwave Technol.* **18** 618
[10] Texeira F L and Chew W C 1998 *IEEE Microw. Guided Wave Lett.* **8** 223
[11] Kim T G, Wang X L, Kaji R and Ogura M 2000 *Physica* E **7** 508
[12] Kapon E, Hardy A and Katzir A 1982 *IEEE J. Quantum Electron.* **18** 66
[13] Champagne A, Maciejko R, Adams D M, Pakulski G, Takasaki B and Makino T 1999 *IEEE J. Quantum Electron.* **35** 1390
[14] Ohira K, Nunoya N and Arai S 2003 *IEEE J. Sel. Top. Quantum Electron.* **9** 1166